

Hybrid Segmentation and Exploration of the Human Lungs

Dirk Bartz¹, Dirk Mayer², Jan Fischer¹, Sebastian Ley², Anxo del Río¹, Steffi Thust², Claus Peter Heussel², Hans-Ulrich Kauczor², and Wolfgang Straßer³

¹Visual Computing for Medicine Group and ³WSI/GRIS
Eberhard-Karls-University Tübingen
Tübingen, Germany*

²Department of Radiology
Johannes-Gutenberg-University Mainz
Mainz, Germany[†]

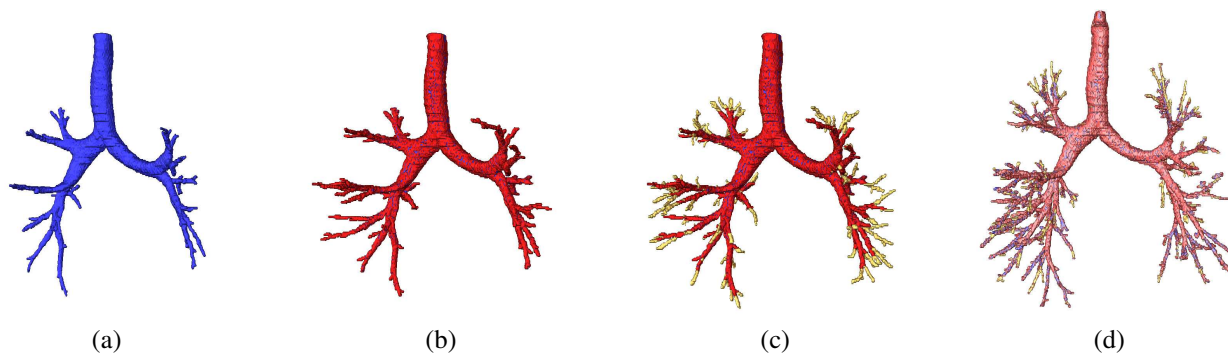


Figure 1: Results of three segmentation stages: (a) Region growing, (b) 2D wave propagation, (c) 2D template matching, (d) final segmentation result after six iterations, taking about 76s on a PC with a P3 @ 850 MHz.

Abstract

Segmentation of the tracheo-bronchial tree of the lungs is notoriously difficult. This is due to the fact that the small size of some of the anatomical structures are subject to partial volume effects. Furthermore, the limited intensity contrast between the participating materials (air, blood, and tissue) increases the segmentation difficulties.

In this paper, we propose a hybrid segmentation method which is based on a pipeline of three segmentation stages to extract the lower airways down to the seventh generation of the bronchi. User interaction is limited to the specification of a seed point inside the easily detectable trachea at the upper end of the lower airways. Similarly, the complementary vascular tree of the lungs can be segmented. Furthermore, we modified our virtual endoscopy system to visualize the vascular and airway system of the lungs along with other features, such as lung tumors.

*{bartz,fischer,anxo}@gris.uni-tuebingen.de

[†]dmayer@radiologie.klinik.uni-mainz.de

CCS Categories: I.3.7 [Three-Dimensional Graphics and Realism]: Virtual Reality; I.3.8 [Application]: Virtual Medicine' J.3 [Life and Medical Sciences]: Pulmology, Radiology'

Keywords: Tracheo-bronchial tree, segmentation, multi-slice CT, virtual endoscopy

1 Introduction

The human body consists of several organ systems which control the numerous body functions. Among them are the metabolism, the circulation of the blood and other body fluids (ie., lymphatic fluids), and the respiratory functions. The latter one transports air into the body (inhaling) and removes exhausted air from the body during the exhale. The exchange of the air takes place in the lungs, which are a complementary system of airways and blood vessels. Both systems are supplied through large pipe-like structures which split successively into smaller ones, thus creating the tracheo-bronchial (airways) and blood vessel tree.

The tracheo-bronchial tree is connected to the outside through the trachea which splits into the main bronchi (left and right lungs) at the main bifurcation. The inhaled air is distributed through the bronchial tree down to the alveoli, where the oxygen/carbon-dioxide exchange between air and blood takes place. The exhausted air (enriched with carbon-dioxide) is then transported back up to the trachea during the exhale. The tracheo-bronchial tree is complemented by a system of pulmonary venous and arterial blood vessels which transports the blood to and from the heart into the lungs.

Several pathologies can jeopardize a sufficient lung function. Among them are tumors, pulmonary embolism, collapse of the lungs (atelectasis), pneumonia, emphysema, asthma, and many

more. For a proper diagnosis and treatment, the respective pathologies need to be identified and in some cases quantified. In the case of lung-surgery (i.e., for tumor treatment), this information is necessary for the intervention planning where the anatomical relation of diseased bronchi to non-diseased areas is required pre-operatively, i.e. to provide a safe distance to essential structures and to determine resectability. In these cases, virtual bronchoscopy with a representation of the vascular structures is in particular useful to represent the spatial and functional relationship in the target area. Another example of a useful application of virtual bronchoscopy is modeling and simulation of inhaled therapies where the exact amount of drug deposition in the lungs is investigated [COPHIT Consortium n. d.]. Here, virtual bronchoscopy can be used to visualize the local drug deposition in the specific bronchies. Finally, virtual bronchoscopy can be used for the assessment of complex esophagus-trachea syrinx that can be difficult to assess in its 3D relationship with regular 2D imaging.

The current gold-standard to identify the respective lung parenchyma and airways is computed tomography (CT) that is performed prior to a bronchoscopy, a tool for inspections of the trachea and central bronchi and deriving tissue samples. Due to the recent technical development improving resolution and scan velocity, multi-slice CT – in connection with virtual bronchoscopy – became a promising alternative to bronchoscopy, if tissue samples are not required. This is amplified by the fact that optical bronchoscopy is limited by smaller, lower airways (third generation and up) or by obstructions. Nevertheless, even smaller structures of the lower airways are extremely difficult to segment from CT datasets, due to leakages, caused by the notorious partial volume effect and due to the lack of sufficient contrast to surrounding tissue or air. However, note that the clinical benefits of virtual bronchoscopy are in principle limited to the data acquisition techniques; features that cannot be detected by it (here multi-slice CT), can also not be exposed by virtual bronchoscopy. Furthermore, the add-on value of a virtual bronchoscopy in contrast to the CT imaging for tumor diagnosis is still disputed.

In this contribution, we introduce a hybrid segmentation method which is based on a pipeline of three segmentation stages to extract the lower airways up to the seventh generation of the lungs (with decreasing sensitivity), starting with the trachea as generation zero. User interaction is limited to the specification of a seed point inside the easily detectable upper airways¹. Similarly, the complementary vascular tree of the lungs can be segmented. Furthermore, we modified our virtual endoscopy system [Bartz et al. 2001] to visualize the vascular and airway system of the lungs along with other features, such as lung tumors, from an endoscopic point of view.

In the following parts of this paper, we briefly review related work in the fields of virtual bronchoscopy and segmentation of the airways in the next section. Afterwards, we will introduce the hybrid segmentation method, including all its pipeline stages in Section 2.1. After briefly describing the modified virtual endoscopy system (Section 2.6), we present our results and an evaluation of the segmentation quality for a diverse set of datasets from healthy subjects, and subjects who are suffering from diseases of the lungs (Section 3). Finally in Section 4, we present some conclusions and point to future research directions.

1.1 Related Work

Virtual endoscopy is currently one of the most popular research fields in medical imaging and is slowly moving into the clinical routine. Considering the extensive work developed in the last years on the field of virtual endoscopy, here we will limit ourselves to describe only that work which is directly related to virtual bronchoscopy.

¹Other parameters are pre-defined and can be modified by the users.

The application of virtual endoscopic techniques to the airways, has been proposed since 1994 [Vining et al. 1994; Mori et al. 1994]. Typically it uses helical CT as imaging modality which provides short acquisition times and thus minimizes the motion artifacts due to breathing and heart beating [Rodenwaldt et al. 1997]. The rendering of the volumetric data can be performed through two common ways: shaded surface rendering (polygonal rendering) and (direct) volume rendering [Remy et al. 1998]. For shaded surface rendering, a polygonal representation of the surface must be extracted from the volume data. Most of the approaches to virtual endoscopy in general and virtual bronchoscopy in particular, make use of threshold-based region growing methods as basic segmentation technique to obtain the surface voxels [Summers et al. 1996; Remy et al. 1998; Mori et al. 1998; Ferretti et al. 2001] Once the surface has been identified, the polygonal representation is generated with the Marching Cubes algorithm [Lorenson and Cline 1987]. However, with these techniques and due to the complexity of the bronchial structure, only the upper bronchi could be properly segmented [Summers et al. 1996]. Law and Heng use a combination of region growing and centerline extraction to enhance the understanding of the 3D structure of the bronchial tree [Law and Heng 2000]. More recently, Kiraly et al. use a combination of an adaptive 3D region growing, 2D mathematical morphology, and an optional 2D median filter for increasing the robustness of the segmentation algorithm while improving the quality of the results [Kiraly et al. 2002]. Also recently, Kitasaka et al. used a regular region growing approach and controlled leaking and bifurcation problems by a complex use of local volume of interest templates that limit the region growing area [Kitasaka et al. 2002].

In contrast, Rodenwaldt et al. adopted a different approach for the reconstruction of the 3D surface from CT data [Rodenwaldt et al. 1997]. They use the “Navigator” software program (GE Medical Systems, Buc, France), which employs a threshold-based modified ray casting technique to determine and render the walls of the inner lumen. Also Fung and Heng use direct volume rendering through ray casting for their virtual bronchoscopy application [Fung and Heng 1999]. They argue that direct volume rendering has the advantage that no information present in the original data is discarded during a segmentation process. However it comes at the cost of requiring intensive parallel rendering in order to provide interactive frame rates. A different alternative is presented by Wegenkittl et al. where an image based rendering technique is used, based on cubic environment mapping of six video sequences [Wegenkittl et al. 2000]. Although this method produces real time frame rates with a considerable image quality, it is restricted to navigation through a fixed path and presents high pre-processing requirements. During this time intensive pre-processing, the video sequences are computed either using shaded surface rendering, or volume rendering techniques. A further overview of existing visualization techniques applied to airway diseases can be found in [Grenier et al. 2002].

2 Methods for Virtual Bronchoscopy

The segmentation and visualization is based on CT data acquired by a Siemens Somatom Volume Zoom multi-slice CT scanner (acquires four spirals at a time, convolution kernel 50, collimation of 1.25mm and increment of 1mm). For a thorax exam, it typically generates a stack of 250-300 images with a matrix of 512 x 512 pixels resolution and a spacing which varies in the sub-millimeter range (i.e., 0.6mm - 0.7mm) for the pixel distance and 1mm for the slice distance. Based on this dataset, we segment the tracheo-bronchial and the blood vessel tree of the lungs using the segmentation system SegoMeTex, and other structures of interest (i.e., a tumor), if available.

Subsequently, we reconstruct the inner surface of these struc-

tures and generate additional data-structures needed for virtual endoscopy. Finally, we explore the dataset by a virtual bronchoscopy procedure using the VIVENDI system [Bartz and Skalej 1999].

2.1 Segmentation

The segmentation pipeline consists of three stages (Fig. 1 and Fig. 2). In the first stage, the trachea and central bronchi are segmented using standard 3D region growing methods.

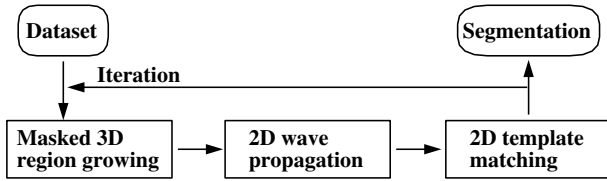


Figure 2: Segmentation pipeline.

Partial volume effects and limited resolution of the CT scan (which essentially cause this effect) render this method as not satisfactory for segmentations of further generations of the bronchi, since bordering voxels cannot be sufficiently differentiated from tissue voxels². Therefore, a 2D wave propagation is initiated to complete the upper and central branches. Finally, a 2D template matching procedure is used to segment small lumen, which might be only a single voxel large. A feedback loop of the whole pipeline repeats the stages until no meaningful additions could be made to the previous segmentation (Fig. 2). Figure 1d shows the final results of five iterations. However, some datasets might require up to 15 iterations.

2.2 Masked 3D Region Growing

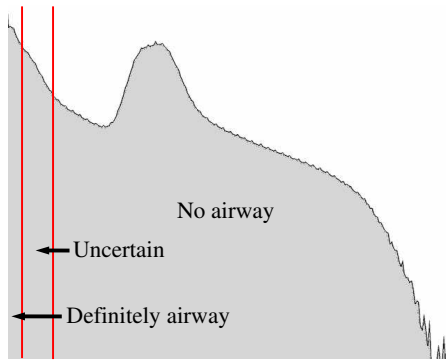


Figure 3: Logarithmic histogram of CT dataset.

If we analyze the histogram of the CT dataset of the thorax, we can differentiate the intensity values in the voxels into three categories (Fig. 3). All values below -950 HU (Hounsfield Units) can be classified as **definitely airway**, and the intensity values above -775 HU as **non-airway**. All voxels values between this isovalue interval (from -950 HU to -775 HU) can possibly belong to airway, thus they are classified as **uncertain**.

²The partial volume effect is averaging low intensity air values with middle intensity bronchi wall or tissue values. The resulting voxel value cannot safely be classified as airway or wall.

Based on this analysis, the 3D region growing algorithm extracts all voxels which are definitely airway, starting at the seed point in the trachea. To prevent the leaking into the parenchyma of the lungs in smaller airways (ie., in emphysema), we use a masking technique from texture analysis; if the average gray value of a $3 \times 3 \times 3$ voxel cube centered at the current voxel is within the save range (below -950 HU), we consider this voxel as being part of the airway. Otherwise, the respective voxel is not classified as airway in this stage. While this masking technique prevents leakage, it also impedes the segmentation of smaller bronchi. However, we usually accomplish the segmentation of the bronchial tree up to the fifth generation, whereas the bordering voxels are often not included, since their voxel values belong to the uncertain voxel value interval (see Fig. 1a/b and Fig. 4).

In the second iteration of the segmentation pipeline, the 3D region growing algorithm runs with the same threshold on the bordering voxels of the previously selected voxels.

2.3 2D Wave Propagation

Starting from segmented voxels of the previous step, 2D wave propagation tries to reconstruct bronchi walls within a single CT slice. It starts at each boundary voxel of the airway voxels from 3D region growing and propagates waves to detect the walls of the bronchi (Fig. 4b). Voxels at position X in the **uncertain** areas are classified by fuzzy logic rules that consider the density value $V(X)$ (in Hounsfield), the largest local N4 neighborhood (in 2D) gradient $G(X)$, and if voxels in the local N4 neighborhood are already classified as wall pixels (no airway) in a previous wave $W(X)$:

$$f_{wave}(X) = c_v * V(X) + c_g * G(X) + c_w * W(X), \quad (1)$$

with $c_v = 1, c_g = 1, c_w = 0.75$.

where $V(X)$ and $G(X)$ are mapped into the closed interval $[1.0, 0.0]$, and $W(X)$ is either 1 – if there is a classified wall pixel in the N4 neighborhood — or 0 – otherwise. Essentially, if $f_{wave}(X) \geq c_{wall}$, the voxel is classified as wall³.

Critical to the wave propagation is the evaluation of the classified airway areas, if they really belong to the airways. To achieve this goal, the additional voxels segmented by each wave are monitored by a protocol that verifies the shape and size of each bronchus candidate, using a set of default parameters (Fig. 4b). As metric, we count the number of voxels selected by the n waves propagating within a plane (BPS_n for BronchusPlainSize), and the wave diameter (WD_n) of the current wave n as the number of selected voxels of wave n. Furthermore, we define the average number of voxels of the first n waves (AWD_n for Average Wave Diameter).

Segments of the tracheo-bronchial tree are identified by sequences of as airway classified voxels in a wave. Figure 4b shows two sequences marked by the red points, thus depicting a bifurcation. The shape rules essentially assume that no wave detects segment splits in more than two subsequent segments at a bifurcation. A third segment (of not yet selected voxels) in one 2D wave propagation test (in one slice) is henceforth considered as leakage into the lungs and is considered invalid. At each bifurcation, the segment identification process starts again recursively.

As closer examination of the datasets showed, two very close bifurcations were never located close enough to be detected as a third segment by the 2D wave propagation, thus they were not falsely

³Typically, $c_{wall} = 1.74$.

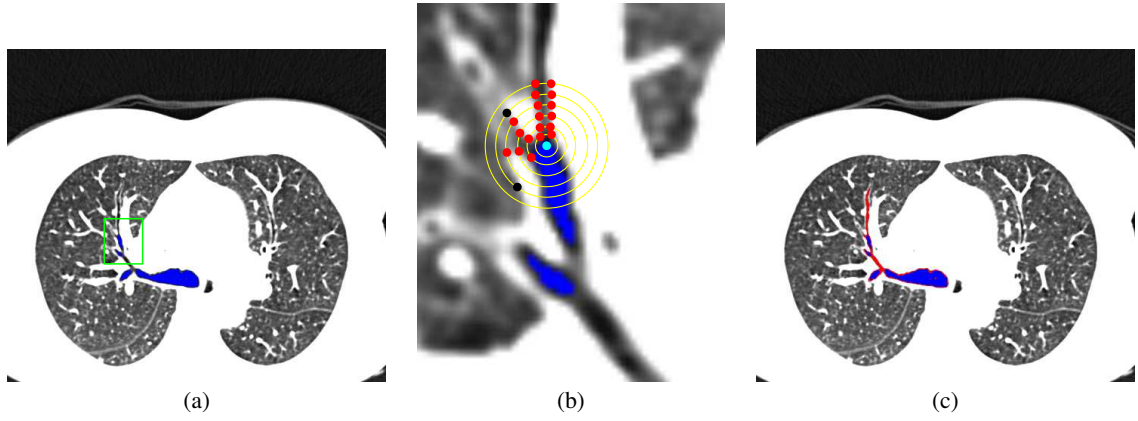


Figure 4: Completion of bronchi walls; (a) shows the result of the 3D region growing (blue). The green rectangle marks the zoomed area shown in (b). (b) shows the wave propagation in progress. The cyan boundary voxel is chosen as starting point. The yellow circles mark the propagated waves and the red points mark the airway candidate voxels. The black points failed the leaking test, since the number of voxels of that wave was increasing too fast. Note that the actual waves have a Rhombus-like shape, driven by the N4-neighborhood. (c) shows the completion of that segmentation by 2D wave propagation (red). The voxels (within the body) in the iso-range of **definitely airway** are marked in blue, of the **uncertain** range in black/grey, and of the **no airway** range in white.

identified as leakage.

$$WD_n > d_{max} \quad (2)$$

$$WD_n / WD_{n-1} > d_{WD_{ratio}} \quad (3)$$

$$BPS_n > d_{size} \quad (4)$$

$$AWD_n - AWD_{n-1} > d_{AWD_{current}} \quad (5)$$

$$AWD_{max} - AWD_{min} > d_{AWD_{longterm}} \quad (6)$$

The size rules limit the growing of the wave propagation⁴. If the diameter of a bronchi candidate exceeds a certain size (Equation 2), or if the wave diameter is increasing too fast from the previous wave (Equation 3, see also black points in Fig. 4b), the respective segment recursion is terminated and the results are considered invalid. Furthermore, if candidates grow spontaneously (while shrinking before) or the overall in plane voxel size BPS_n of the candidate becomes unrealistically large (Equation 4), the recursion is again terminated and the results are set invalid. The last two rules (Eqn. 5 and 6) test the current and long-term growth of the wave front. Specifically, they test if the segments are shrinking (as assumed) or growing. The protocol starts testing after the first three waves, since they frequently show an unstable behavior. During the wave propagation, all invalid results are removed from the segmentation. However, initial correct results (ie., for the first p waves) are preserved.

To follow a bronchus through several slices, virtual waves are propagated in neighboring slices. If one of these virtual waves is similar to the shape and size of the wave propagation in the current slice, another recursive wave propagation in the neighboring slice is initiated. Specifically, the recursive testing of waves in neighboring slice is initiated only for no-branching segments that have classified wall elements from 2D wave propagation. Furthermore, these wall elements may only differ by one voxel to the wall elements of the new neighboring slice segment.

Similar to the first step of the pipeline, 2D wave propagation uses almost the same parameters in the subsequent iteration; only the peripheral bronchi diameter is reduced since the lower airways (higher generations) only grow smaller.

⁴We use $d_{max} = 6.1mm$, $d_{WD_{ratio}} = 1.75$, $d_{size} = 500mm^2$, $d_{AWD_{current}} = 1.13$, $d_{AWD_{longterm}} = 3.0$.

2.4 2D Template Matching

Without the used careful validity testing, the previous two stages would leak into the surrounding area, if the airways become too small to be picked up, in particular in areas where the airways might have the size of only one voxel. To select these voxels, but still prevent the leaking, we apply a 2D template matching technique which evaluates the candidate area below templates with the isovalue category **uncertain** (between -950 HU and -775 HU). This stage is organized in two steps; the first step establishes templates that are used in the second step to evaluate the local voxel neighborhood.

First, 2D template matching applies 2D region growing starting from the boundary voxels of the previous segmentations (Fig. 5). The thresholds are varied – from the upper threshold of the **uncertain** isovalue interval (-775 HU) – until the number of selected voxels is below the critical limit (ie., 35 voxels), since it can be assumed that they did not leak out. Based on this selected voxel area, circular templates of varying sizes are generated.

In the second step, we apply a 2D region growing and use the templates to differentiate the thresholds; below the template, we are using the upper **uncertain** threshold (-775 HU), while we are using the original template threshold outside of the template. By moving the templates over the local area, we generate various segmentation candidates (see Fig. 5b-e) which are again evaluated by a set of fuzzy rules. This time, we consider the average density value $V'(X)$ of the template area and the (filtered⁵) average gradient $G(X)$ to the surrounding voxels in the N8 neighborhood (within a single slice). The best possible result is then selected and added to the segmentation (Fig. 5f and Fig. 1d).

$$f_{template}(X) = c_{ave} * V'(X) + c_{grad} * G(X), \quad (7)$$

with $c_{ave} = 0.25$ and $c_{grad} = 0.75$.

Here, $V'(X)$ is mapped from [-1024,-775] to [0.0,1.0], and $G(X)$ is mapped into the range [0.0, 1.0]. Illustratively, this means that accepted candidates have a low average density value and a high boundary contrast. The candidate with the largest $f_{template} \geq 0.7$ (Eqn. 7) is accepted as airway (Fig. 5f and Fig. 1d).

However, if the size of the template controlled area is larger than twice as much as for the previous slice, a leak-out is assumed, thus

⁵In order to reduce data artifacts, we clamp the gradient range.

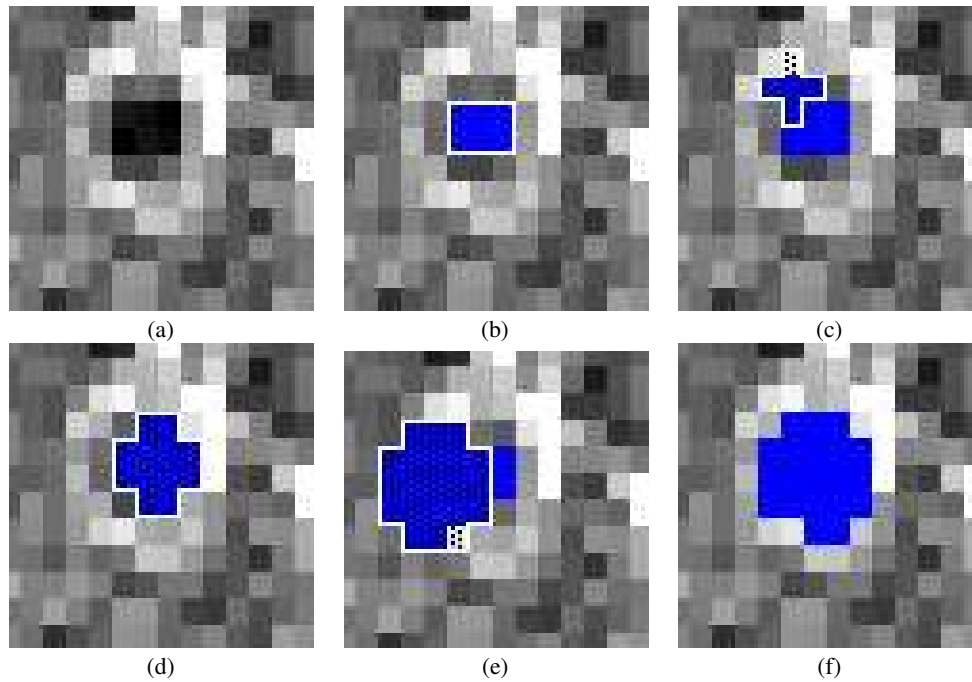


Figure 5: Template matching: (a) shows a peripheral airway. 2D seeding is started on pixels of the category **uncertain**. The result is marked blue (b). From there the seeding area templates (white polygon with black dot pattern) are formed and tested on different locations around the seeding. The seeding is repeated on the category uncertain and template (marked by a pattern, (c) to (e)). (f) shows the best result after the classification.

the area of the current slice is assumed invalid.

In the subsequent iterations, voxels which have already been unsuccessfully tested for inclusion, are excluded from template matching. This is mainly to save time – 2D template matching is the single most time consuming stage of the segmentation pipeline – and they usually do not contribute in later iterations.

2.5 Segmenting Blood Vessels

To segment the blood vessels, we are using the same three stage segmentation pipeline, based on a dataset that was scanned while injecting a iodine-based contrast agent to enhance the contrast of the blood filled vessels to the neighboring tissue. In addition, the lower (**definitely airway**) and upper (**no airway**) thresholds are adapted to the intensity values of the contrast agent filled blood vessels (130 HU, 250 HU). Note that this time we are looking for a higher intensity structure, in contrast to the very low intensity of the airways.

Similar to the tracheo-bronchial tree, the pulmonary artery tree has the tendency that its diameter is decreasing while descending to the arteriole level of the arterial tree. If the segmentation proceeds to the complementary venous vessel tree, the diameter will increase again, triggering the leakage detectors of the segmentation pipeline. Thus, only the arterial tree is segmented. However, the varying quality of the contrast agent distribution in the blood vessels causes also a varying quality of its segmentation. Therefore, no fixed Hounsfield thresholds – in contrast to the airway segmentation – can be used; they need to be adapted to the specific datasets. Furthermore, additional manual editing may be required to achieve the necessary quality (see also Section 3 and Fig. 8c).

2.6 Virtual Endoscopy

Based on the generated segmentation, we reconstruct the iso-surface of the segmentation (see Fig. 7c) using the standard Marching Cubes algorithm [Lorensen and Cline 1987]. Here we use the segmentation as a template to restrict the iso-surface extraction to the volume cells that contain segmented voxels. However, the direct reconstruction from a (binary) segmentation can result in a bumpy appearance, caused by interpolation artifacts due to high density differences between the voxels of the segmentation and the not selected surrounding voxels. Therefore, we add one layer/shell of voxels to the boundary voxels of segmentation that reduces this effect. The application of more continuous distance fields can further reduce this effect. However, it might also reduce reconstructed segmentation details. In some cases (ie., 7th generation bronchi in Fig. 7c), this can result into holes that are clearly visible from the outside, but negligible for most of the interior viewpoints. A fall-back to the binary segmentation template can reduce this artifact.

For the virtual endoscopic exploration, we use the reconstructed models (ie., tracheo-bronchial tree and pulmonary blood vessel tree) and render those independently. Usually, we assume a viewpoint inside a bronchus, hence we render its surface semi-transparent and the pulmonary vessels opaque. However, we can also assume a viewpoint inside the blood vessels. Consequently, the transparency parameters would be switched. Independently from the chosen viewpoint location, the enclosing structure is rendered semi-transparent, while the outside structure should be rendered opaque. Note that also other structures (i.e., a tumor) can be added to the scene. In this case, the rendering parameters need to be chosen accordingly.

To determine the visibility of the scene components (tracheo-bronchial tree, pulmonary arteries, and tumor(s)), we render the front-to-back sorted opaque components using visibility driven rendering algorithm as described in [Bartz and Skalej 1999], where

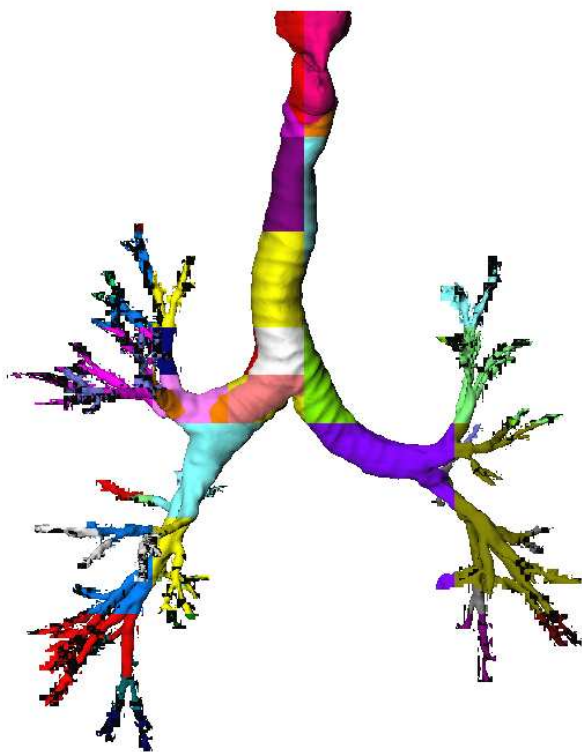


Figure 6: Reconstruction of iso-surface of dataset 2. The different octree leaf blocks are coded in different colors.

we use an octree-based scene decomposition to organize the scene in hierarchical octree blocks, in which the leaf blocks contain the actual scene geometry (see Fig. 6 and Table 1). Finally, the semi-transparent component – usually the tracheo-bronchial tree – is rendered. If we use the mentioned visibility driven rendering for this component, we trade off rendering quality⁶ and rendering speed [Bartz et al. 2001].

For the actual virtual bronchoscopy, we start in the trachea (Fig. 7a) and traverse the tracheo-bronchial tree (Fig. 7b) to the target region of interest. Interesting structures or pathologies can be documented for further evaluation. As we will show in the next section, we traverse the tracheo-bronchial tree and see the pulmonary arteries and a tumor of the lungs (Fig. 8).

We choose an indirect volume rendering technique for our visualization component due to the required high sustained, full quality rendering performance of more than 30fps. Therefore, we did not use any mesh reduction approach, but visibility driven rendering.

For the same reasons, we opted against a direct volume rendering approach that might be able to generate higher quality images. A texture-mapping-based volume rendering approach will also encounter severe memory problems, since the label (segmentation) volume and the volume dataset itself are required for the proper rendering. Finally, note that in contrast to a common misconception, we still need a segmentation pipeline for the successful segmentation of the structures of interest; a classification by (multi-dimensional) transfer functions is not able to differentiate between the low intensity airways, the empty space between the airways in

⁶The occlusion culling part of the visibility calculation assumes opaque rendering. If we nevertheless render components semi-transparent, we will experience minor popping artifacts [Bartz et al. 2001].

the lungs, and the space outside of the body.

3 Results

The segmentation method was successfully tested on datasets from 22 patients (approximately 6600 dataset slices), who were separated into three groups of normal subjects (n=8), emphysema (n=5), and lung diseases with increased density, such as pneumonia (n=9). The results of the segmentation were compared to segmentations using only the threshold/region growing method – which is still the widely used state-of-the-art for segmentation of the tracheo-bronchial tree – and assessed by an experienced chest radiologist, who also identified false positive segmentation results⁷.

The reliability of the segmentation is statistically measured by the sensitivity and the positive predictive value. The sensitivity describes how reliable those bronchi branches are correctly found (correctly found bronchi branches / existing bronchi branches detected by the radiologist). In contrast, the positive predictive value (PPV) describes the accuracy that **only** existing bronchi branches are detected by the segmentation pipeline (correctly found bronchi branches / (correctly found bronchi branches + found false positive bronchi branches)). Therefore, one can interpret the PPV as the specificity (which describes the reliability that negative cases are detected as negative) of leaked (invalid) bronchi branches. The actual specificity could not be determined, since the number of “correct negative” bronchies (no bronchies) cannot be measured.

The presented hybrid segmentation method identified bronchi up to the fifth generation with a sensitivity of more than 85%, up to the sixth generation with a sensitivity of more than 58%, and a PPV of more than 90%. Beyond the sixth generation, the sensitivity drops just below 30%, while the PPV maintains its high level. For emphysema patients, the PPV was slightly reduced due to the damage of the alveoli which increased the leakings into false positive branches. For pneumonia patients, the sensitivity (and to a smaller extent the PPV) are significantly reduced compared to the other datasets. This is due to the increased density in the airways which increases the difficulties of tracking the inner surface tremendously.

While almost all parameters (propagation diameter, etc.) are pre-specified – except the seed point –, they can be optimized for individual datasets. However, the segmentation result is only slightly improved compared to the “standard” setting. We consider this as stability feature of our segmentation approach.

Two of the segmentation pipeline stages are working only on individual slice images. Consequently, the identification of structures which grow orthogonal to the slices is not always possible in the same iteration. As it turns out, however, the masked 3D region growing of the next iteration – followed by the other 2D pipeline stages – is able to compensate for this effect. As noted before, usually five to seven iterations are sufficient for a segmentation of the tracheo-bronchial tree, which is usable in our application context. Only in few cases – i.e., like the previously mentioned pathological cases –, the algorithm requires up to 15 iterations. Overall, a typical segmentation process takes between 20 and 100 seconds on a PC with an Intel PIII CPU running at 850MHz. A breakdown of this this time can be found in Table 1.

The iso-surface extraction for dataset 1 (shown in Figure 7) generated 1.1M triangles for the tracheo-bronchi tree and 822K triangles for the pulmonary artery tree (Table 1). In contrast, the polygonal complexity of the dataset 2 (Figure 8) is significantly smaller, mostly due to less refined segmentation results in the upper generations; the tracheo-bronchi tree consists of less than 300K triangles, the pulmonary artery tree of 340K triangles, and the tumor of only

⁷Usually, an experienced radiologist can identify the tracheo-bronchial tree up to the eighth generation.

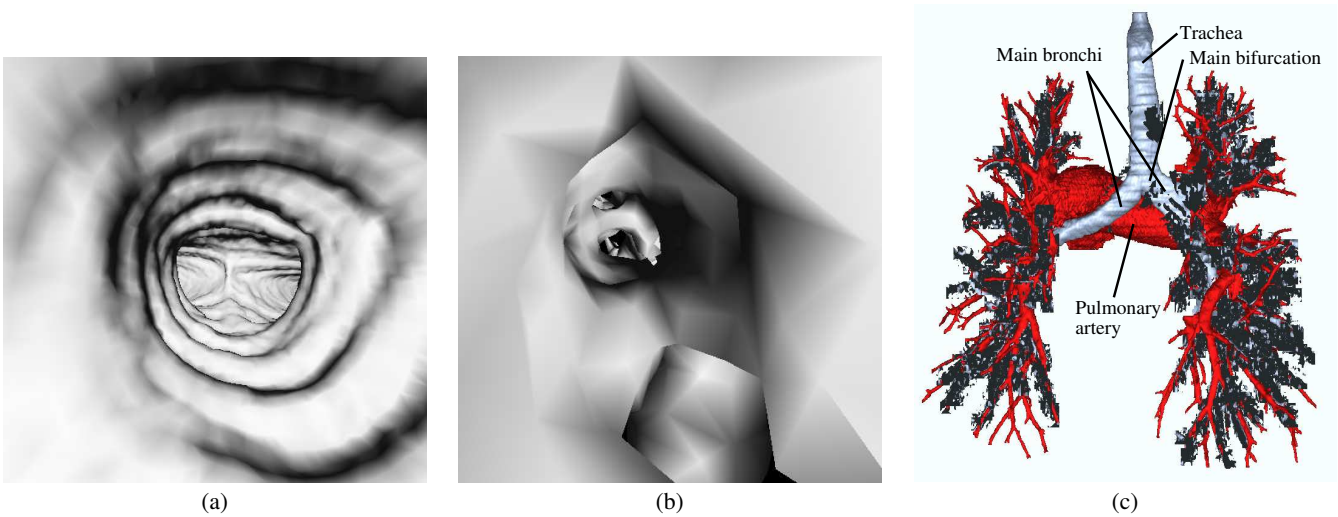


Figure 7: Virtual endoscopy of dataset 1: (a) View in trachea down to main bifurcation, (b) approximately the seventh generation of the lower airways, mainly segmented by 2D template matching. The diamond shape interpolation artifacts are due to high zoom factor in this close-up. They are very typical for Marching Cubes reconstructed iso-surfaces close to the dataset resolution (c) shows an annotated outside representation with the tracheo-bronchial tree (grey) and pulmonary arteries (red) from a view behind the patient body (left image side is left patient side).

Model Complexity	# Polygons	# Octree Leaf Blocks
Tracheo-bronchial Tree	1,148,032	222
Pulmonary Artery Tree	822,906	116
Segmentation Pipeline	Time	# Voxels [%]
Masked 3D Region Growing	3%	70
2D Wave Propagation	11%	27
2D Template Matching	86%	3
Total Segmentation Costs	76s	100
Rendering Performance	Frames per Second	
Opaque Display	53	
Transparent Display	36	

Table 1: Breakdown of typical scene complexity, segmentation and rendering costs (dataset 1). Note that due to organizational reasons the timings for the segmentation were generated on a PC with a P3 @ 850 MHz, while the rendering was performed on a PC with a P4 @ 2.8 GHz.

44K triangles. Since we successfully apply a visibility driven rendering approach (Section 2.6), we achieve a sufficient rendering performance of the full resolution polygon models.

After the segmentation, we explored a subset of the 22 datasets interactively (more than 30fps on a standard PC⁸, see also Table 1) using the virtual endoscopy software [Bartz and Skalej 1999]. The exploration exposed a high quality reconstruction, even of small structures throughout the dataset. In Figure 7, we show two snapshots from a regular virtual bronchoscopy. The left image (Fig. 7a) shows the endo-view from the trachea looking down to the main

⁸In the full opaque mode, a Linux PC equipped with an P4 CPU running at 2.8GHz and an ATI Radeon 9700Pro graphics accelerator rendered more than 1.1M triangles (tracheo-bronchial tree is visible only) at 53fps. In the semi-transparent mode, it achieved 36fps rendering the tracheo-bronchial and the pulmonary artery trees of almost 2M triangles. All geometry is arranged in triangle strips, compiled in OpenGL display lists.

bifurcation, where the tracheo-bronchial tree splits into the left and right lungs. Figure 7b shows the limits of the currently possible segmentation; the virtual endoscope is located approximately in the seventh generation of the lower airways. Due to the high zoom-factors, the typical diamond-shape interpolation artifacts of trilinear interpolation on the voxel cell grid are exposed. Blood vessels were visualized to provide more context information (Fig. 7c).

In Figure 8, we show a more complex situation, where the surrounding arterial blood vessels are visible through the inner surface of the tracheo-bronchial tree. Figure 8c shows a tumor in the right lung in green. At the same time, poor contrast and beam hardening artifacts of the voxels of the pulmonary arteries expose segmentation difficulties; the blood vessel tree is only incompletely segmented (Fig. 8c).

4 Conclusions and Future Work

In this contribution, we discussed a novel segmentation algorithm which consists of a pipeline of three segmentation stages. The segmentation results were combined with VIVENDI, a virtual endoscopy system to provide a (virtual) bronchoscopic exploration mode. Based on a high-quality segmentation, meaningful features could be visualized. Whereas the segmentation provided good results for a large variety of patients, it encountered problems identifying all airways with pneumonia patients, or pulmonary blood vessel structures.

Virtual bronchoscopy is a valuable tool for the localization and measurement of stenosis for treatment planning. However, mild stenosis, submucosal infiltration, and superficial spreading tumors cannot be identified, since they are usually not picked up by the CT data, and hence they are not visualized through the virtual endoscopy system.

Future Work

Future work will focus on the extension of the last two pipeline stages into 3D. While we do not expect a better segmentation result,

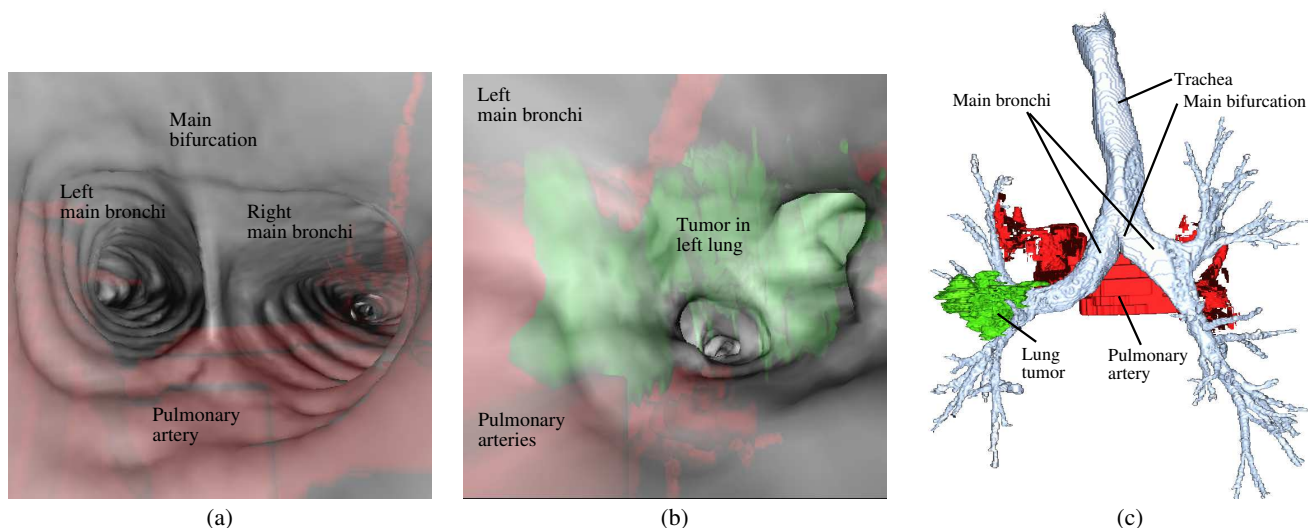


Figure 8: Virtual endoscopy of dataset 2: (a) Semi-transparent rendering of view in trachea at main bifurcation. The pulmonary arteries (red) are visible through the inner surface of the tracheo-bronchial tree. (b) shows the same situation further down the bronchi. The tumor (green) encloses the bronchi (grey). (c) shows an annotated outside representation of another dataset with the tracheo-bronchial tree (grey), pulmonary arteries (red), and a lung tumor (green) in the left lung (view from behind the patient).

3D operations will reduce the number of required iteration steps, thus it will reduce the required time. Furthermore, we are looking into improving the stability of the algorithms for datasets with poor tissue contrast, like the blood vessels in Figure 8.

ACKNOWLEDGEMENTS

This work was supported by the European Commission (IST-1999-14004: "COPHIT", the DAAD/British Council, and by DFG Projects CatTrain and Virtue. We would like to thank Özlem Gürvit of the University Hospital Marburg for helpful discussions and Mike Doggett of ATI providing the most recent Linux drivers for the Radeon 9700Pro in time. Finally, we thank Urs Kanus for proof-reading.

References

BARTZ, D., AND SKALEJ, M. 1999. VIVENDI - A Virtual Ventricle Endoscopy System for Virtual Medicine. In *Proc. of Symposium on Visualization*, 155–166,324.

BARTZ, D., STRASSER, W., GÜRVIK, O., FREUDENSTEIN, D., AND SKALEJ, M. 2001. Interactive and Multi-modal Visualization for Neuroendoscopic Interventions. In *Proc. of Symposium on Visualization*, 157–164.

COPHIT CONSORTIUM. EU COPHIT Project: Computer-Optimised Pulmonary Delivery in Humans of Inhaled Therapies. <http://www.cophit.co.uk>.

FERRETTI, G., BRICAULT, I., AND COULOMB, M. 2001. Virtual Tools for Imaging of the Thorax. *European Respiratory Journal* 18, 381–392.

FUNG, P., AND HENG, P. 1999. High Performance Computer Simulated Bronchoscopy with Interactive Navigation. In *Proc. of Computer Aided Radiology and Surgery*, 161–165.

GRENIER, P., BEIGELMAN-AUBRY, C., FETITA, C., PRETEUX, F., BRAUNER, M., AND S. S. L. 2002. New Frontiers in CT Imaging of Airway Disease. *European Radiology* 12, 5, 1022–1044.

KIRALY, A., HIGGINS, W., MCLENNAN, G., HOFFMAN, E., AND REINHARDT, J. 2002. Three-Dimensional Human Airway Segmentation Methods for Clinical Virtual Bronchoscopy. *Academic Radiology* 9, 10, 1153–1168.

KITASAKA, T., MORI, K., HASEGAWA, J., AND TORIWAKI, J. 2002. A Method for Extraction of Bronchus Regions from 3D Chest X-ray CT Images by Analyzing Structural Features of the Bronchus. *Forma* 17, 4, 321–338.

LAW, T., AND HENG, P. 2000. Automatic Centerline Extraction for 3D Virtual Bronchoscopy. In *Proc. of MICCAI*, 786–795.

LORENSEN, W., AND CLINE, H. 1987. Marching Cubes: A High Resolution 3D Surface Construction Algorithm. In *Proc. of ACM SIGGRAPH*, 163–169.

MORI, K., HASEGAWA, J., TORIWAKI, J., YOKOI, S., ANNO, H., AND KATADA, K. 1994. A Method to Extract Pipe Structured Components in Three Dimensional Medical Images and Simulation of Bronchus Endoscope Images. In *Proc. of 3D Image Conference*, 269–274.

MORI, K., HASEGAWA, J., SUENAGA, Y., TORIWAKI, J., ANNO, H., AND KATADA, K. 1998. Automated Labeling of Bronchial Branches in Virtual Bronchoscopy System. In *Proc. of MICCAI*, 870–878.

REMY, J., REMY-JARDIN, M., ARTAUD, D., AND FRIBOURG, M. 1998. Multiplanar and Three-dimensional Reconstruction Techniques in CT: Impact on Chest Diseases. *European Radiology* 8, 335–351.

RODENWALDT, J., KOPKA, L., ROEDEL, R., MARGAS, A., AND GRABBE, E. 1997. 3D Virtual Endoscopy of the Upper Airways: Optimization of the Scan Parameters in a Cadaver Phantom and Clinical Assessment. *Journal of Computer Assisted Tomography* 21(3), 405–411.

SUMMERS, R., FENG, D., HOLLAND, S., SNELLER, M., AND SHELLHAMER, J. 1996. Virtual Bronchoscopy: Segmentation Method for Real-Time Display. *Radiology* 200, 857–862.

VINING, D., SHIFRIN, R., HAPONIK, E., LIU, K., AND CHOPLIN, R. 1994. Virtual Bronchoscopy (abstract). In *Radiology*, vol. 193(P), 261.

WEGENKITTL, R., VILANOVA, A., HEGEDÜS, B., WAGNER, D., FREUND, M., AND GRÖLLER, E. 2000. Mastering Interactive Virtual Bronchoscopy on a Low-End PC. In *Proc. of IEEE Visualization*, 461–465.